

Advanced Two-Moment Bulk Microphysics for Global Models. Part II: Global Model Solutions and Aerosol–Cloud Interactions*

A. GETTELMAN, H. MORRISON, S. SANTOS, AND P. BOGENSCHUTZ

National Center for Atmospheric Research,⁺ Boulder, Colorado

P. M. CALDWELL

Lawrence Livermore National Laboratory, Livermore, California

(Manuscript received 31 January 2014, in final form 29 August 2014)

ABSTRACT


A modified microphysics scheme is implemented in the Community Atmosphere Model, version 5 (CAM5). The new scheme features prognostic precipitation. The coupling between the microphysics and the rest of the model is modified to make it more flexible. Single-column tests show the new microphysics can simulate a constrained drizzling stratocumulus case. Substepping the cloud condensation (macrophysics) within a time step improves single-column results. Simulations of mixed-phase cases are strongly sensitive to ice nucleation. The new microphysics alters process rates in both single-column and global simulations, even at low (200 km) horizontal resolution. Thus, prognostic precipitation can be important, even in low-resolution simulations where advection of precipitation is not important. Accretion dominates as liquid water path increases in agreement with cloud-resolving model simulations and estimates from observations. The new microphysics with prognostic precipitation increases the ratio of accretion over autoconversion. The change in process rates appears to significantly reduce aerosol–cloud interactions and indirect radiative effects of anthropogenic aerosols by up to 33% (depending on substepping) to below 1 W m^{-2} of cooling between simulations with preindustrial (1850) and present-day (2000) aerosol emissions.

1. Introduction

To simulate climate and climate change, a proper representation of radiative forcing is necessary. This is surprisingly hard to achieve, largely because of significant uncertainties in anthropogenic forcing due to interactions between clouds and aerosols (Solomon et al. 2007). The heart of the uncertainty is that anthropogenic aerosols alter cloud drop and ice number concentrations, creating important changes in the radiative properties of clouds

(Twomey 1977) and the formation of precipitation and cloud lifetime (Albrecht 1989). For simulating these changes, a complex series of processes must be represented, from aerosol formation and evolution to activation of cloud drops to cloud microphysics. In global climate models, this is a challenging task since the scale of cloud motions is very much smaller than the typical model grid scale of 50–200 km. These processes therefore must be parameterized.

The representation of cloud microphysics and aerosol interactions has advanced significantly in global models over the last decade. New representations of microphysics schemes now consistently represent the mass and number concentrations of cloud drops (Lohmann et al. 1999) and ice crystals (Morrison and Gettelman 2008, hereafter MG2008), using methods similar to those developed for mesoscale models (Morrison et al. 2005; Thompson et al. 2008; Milbrandt and Yau 2005). Aerosols are also treated by describing multiple modes (Liu et al. 2012), and global models use more physical representations of the activation of cloud condensation nuclei (Abdul-Razzak and

 Denotes Open Access content.

* Supplemental information related to this paper is available at the Journals Online website: <http://dx.doi.org/10.1175/JCLI-D-14-00103.s1>.

⁺ The National Center for Atmospheric Research is sponsored by the National Science Foundation.

Corresponding author address: A. Gettelman, National Center for Atmospheric Research, 1850 Table Mesa Dr., Boulder, CO 80305.
E-mail: andrew@ucar.edu

DOI: 10.1175/JCLI-D-14-00103.1

Ghan 2000; Ghan et al. 2011) and ice nuclei (Kärcher et al. 2006; Liu et al. 2007).

Despite these advances, the sensitivity or “susceptibility” (Platnick and Twomey 1994) of clouds and precipitation to aerosols in GCMs is very different from a sensitivity deduced from observations (Quaas et al. 2009) or from idealized models (Gettelman et al. 2013). In particular, GCMs seem to overpredict aerosol sensitivity. Posselt and Lohmann (2008) suggested that one cause of exaggerated aerosol sensitivity in GCMs is the diagnostic treatment of precipitation at long time steps. Posselt and Lohmann (2008) showed that switching from diagnostic to prognostic rain in a GCM increased the ratio of accretion to autoconversion. Because GCMs tend to parameterize autoconversion but not accretion as dependent on cloud droplet number (e.g., Khairoutdinov and Kogan 2000), increasing the strength of accretion relative to autoconversion is expected to reduce aerosol susceptibility (Gettelman et al. 2013). The dominance of autoconversion means a larger impact of changes in drop number on the warm rain formation process, and on cloud lifetime.

This promise of improved aerosol sensitivity motivates the investigation of prognostic precipitation described in this study. Prognostic precipitation is also expected to improve high-resolution simulations where the diagnostic precipitation assumptions of steady state and neglect of precipitation advection become untenable. We leave a detailed discussion of resolution sensitivity to a future study. As shown below, prognostic precipitation has a large impact on model solutions even when the model horizontal and temporal resolutions imply that advection of precipitation water is negligible. The intent is to look at interactions between precipitation and microphysical processes and large-scale condensation, and not the necessity of prognostic precipitation at higher horizontal resolutions and shorter time steps for advection. Resolution dependence and advection of precipitation will be treated in future work.

This work will extend that of Posselt and Lohmann (2008) and Posselt and Lohmann (2009) by looking in more detail at the coupling between large-scale condensation (macrophysics) and microphysics. Recently, similar approaches have been implemented in the Met Office Unified Model as described by Walters et al. (2014), where it improved the representation of light rain.

In this study, we will document an update to the MG2008 microphysics scheme specifically designed to address aerosol sensitivity in a global climate model. Part I of this work (Gettelman and Morrison 2014, hereafter Part I) describes the scheme and detailed offline numerical tests, including comparison with other schemes. This work will describe the implementation in

the Community Atmosphere Model (CAM), version 5 (CAM5), with single-column and global results. CAM5 is the atmospheric component of the Community Earth System Model (CESM). The analysis includes a detailed description of how the scheme is coupled into the large-scale model. Part II is organized as follows. Section 2 describes the model and methodology. Section 3 presents single-column model results. Section 4 presents global simulations. Conclusions are in section 5.

2. Methods

a. GCM description

The model used is the National Center for Atmospheric Research (NCAR) and Department of Energy (DOE) Community Earth System Model. The atmospheric component (CAM5) is version 5.3. The model is essentially the same as the CAM5.0 model described by Neale et al. (2010). It features two-moment cloud microphysics (MG2008) as implemented by Gettelman et al. (2010). The microphysics are coupled to a three-mode Modal Aerosol Model (MAM3; Liu et al. (2012)) by droplet activation (Abdul-Razzak and Ghan 2000) and ice nucleation (Liu et al. 2007). CAM5.3 also has a separate moist turbulent boundary layer scheme (Bretherton and Park 2009), a shallow convective parameterization (Park and Bretherton 2009), and a deep convective scheme (Zhang and McFarlane 1995) with modifications by Neale et al. (2008). Note that the microphysics in deep and shallow convective clouds is different (single-moment bulk representations). In addition, we will also perform tests with a different moist turbulence and large-scale condensation scheme, the Cloud Layers Unified by Binormals (CLUBB) scheme, originally developed by Golaz et al. (2002) and implemented in CAM5 as described by Bogenschutz et al. (2012). CLUBB replaces the standard boundary layer (Bretherton and Park 2009), large-scale condensation (macrophysics), and shallow cumulus scheme (Park and Bretherton 2009) in the standard version of CAM5. With CLUBB, the microphysics is double moment for stratiform and shallow convective regimes, but single moment for the deep convective regime.

b. Scheme description

We use the microphysical scheme described in Part I, termed MG2. This is an update to the scheme in MG2008 (hereafter MG1). To isolate the effects of (a) prognostic precipitation and (b) substepping we use as a control case an updated version of MG1 termed MG1.5. As described in Part I, MG1.5 is a refactoring of MG2008 (MG1) to be more portable across models and computer architectures and more modular, and to improve computational

performance. MG1.5 contains only one change from MG1 that significantly affects results: updating number concentrations from activated number at the beginning of the microphysics. MG1.5 does not contain prognostic precipitation. The microphysical process rate formulations other than precipitation are the same in MG1.5 and MG2, so differences in the simulations are solely due to differences in the treatment of precipitation. For MG2 the major new scientific feature is the use of prognostic equations for precipitating hydrometeors: rain and snow. Two moments (mass and number mixing ratios) are prognosed and advected for each species. Maximum overlap of clouds in the vertical is assumed when precipitation fraction is estimated. We have also included the evaporation of precipitation number, which was not accounted for by MG1 but can now be tracked as part of prognostic precipitation. We have tested MG2 with and without the evaporation of rain number, and it does not change the conclusions of this study. The code is open source, and is freely available as part of CESM and is available as supplemental material at the Journals Online website: <http://dx.doi.org/10.1175/JCLI-D-14-00103.s1>.

Part I demonstrates the performance of the MG2 scheme in an offline framework. MG2 is able to reproduce results from the original Morrison et al. (2005) scheme for warm rain cases. Using a kinematic driver framework, Part I demonstrates that MG2 is less sensitive to time step size and vertical level structure than MG1.5. Part I tested the scheme with time steps from 1 to 900 s and vertical resolutions from 25 to 500 m in the lower atmosphere (up to 3 km altitude). The MG2 scheme with prognostic precipitation substantially increases the ratio of accretion to autoconversion relative to MG1.5 with diagnostic precipitation. Part I also found that MG2 performs very similarly to other two-moment schemes designed for mesoscale models, such as Morrison et al. (2005) and Thompson et al. (2008).

c. Microphysics time stepping

Cloud microphysical processes often occur on time scales shorter than the 5–30-min time steps employed by GCMs. For example, rain fall speeds often reach 5 m s^{-1} , which require a time step of 100 s for CFL stability with the 500-m grid spacings common to GCMs for calculating sedimentation in MG2. We handle this by substepping¹ sedimentation as needed to maintain stability. Note that these requirements for numerical stability associated with the CFL number of falling precipitation do not apply to MG1 and MG1.5 since they

have a diagnostic treatment of precipitation. While not stability-constrained in the same way, other microphysical processes require a shorter time step for accuracy. In MG1 this is handled through the addition of a substepping layer around a subset of microphysical processes. In MG1.5 and MG2, we extend this additional substepping layer to encompass all of the microphysics code.

Since microphysics generally depletes condensate, the simple forward-Euler time integration scheme used by all incarnations of MG (and nearly all microphysics schemes) tends to overpredict depletion. For long time steps this can result in all liquid condensate (Q_c) being depleted within a single time step (Fig. 1a). Our use of substepping is designed to reduce this error (Fig. 1b) and can result in a very different solution. More sophisticated time integration schemes could also alleviate these problems and will be pursued in a future study.

Further issues arise from the coupling between microphysics and macrophysics. Macrophysics (which refers to the combination of cloud fraction and large-scale condensation parameterizations) is the main source of cloud liquid for microphysics. In CAM5 macrophysics and microphysics are “sequentially split” in the sense that macrophysics is computed first and its impact is applied to the model state passed to microphysics. For the long time steps commonly employed by GCMs, splitting macrophysics and microphysics in this way can deplete all Q_c at one time step (Fig. 1c). In simulations, this typically results in more condensation at the next time step, which is depleted again in a third time step, resulting in an oscillation between cloud and no cloud states. Putting an additional level of substepping around both macrophysics and microphysics reduces this splitting error (Fig. 1d).

In all, we implement three nested layers of substepping: sedimentation, microphysics, and macrophysics. Sedimentation is substepped just enough as needed to satisfy the CFL condition while the impact of varying the number of substeps in the other two processes is explored further below. Table 1 lists the substepping configurations explored in this study. Substeps are denoted “Mi” for microphysics and “Ma” for macrophysics. Note that Mi4Ma1, Mi2Ma2, and Mi1Ma4 all have four microphysics substeps per time step because macrophysics substeps occur at a level that includes microphysics as well as macrophysics. The default behavior in MG1.0 is to substep most microphysics processes twice. For consistency, the base versions of MG1.5 and MG2 also use two microphysics substeps (but with substeps extending over *all* microphysics processes as discussed earlier). Thus, in the notation of Table 1, our base configuration is Mi2Ma1: two microphysics steps (Mi2) and one macrophysics step (Ma1).

¹ When we say we use N substeps of a given process, we mean that we have looped over that process N times using a time step which is N times smaller than used by the rest of the model physical parameterizations.

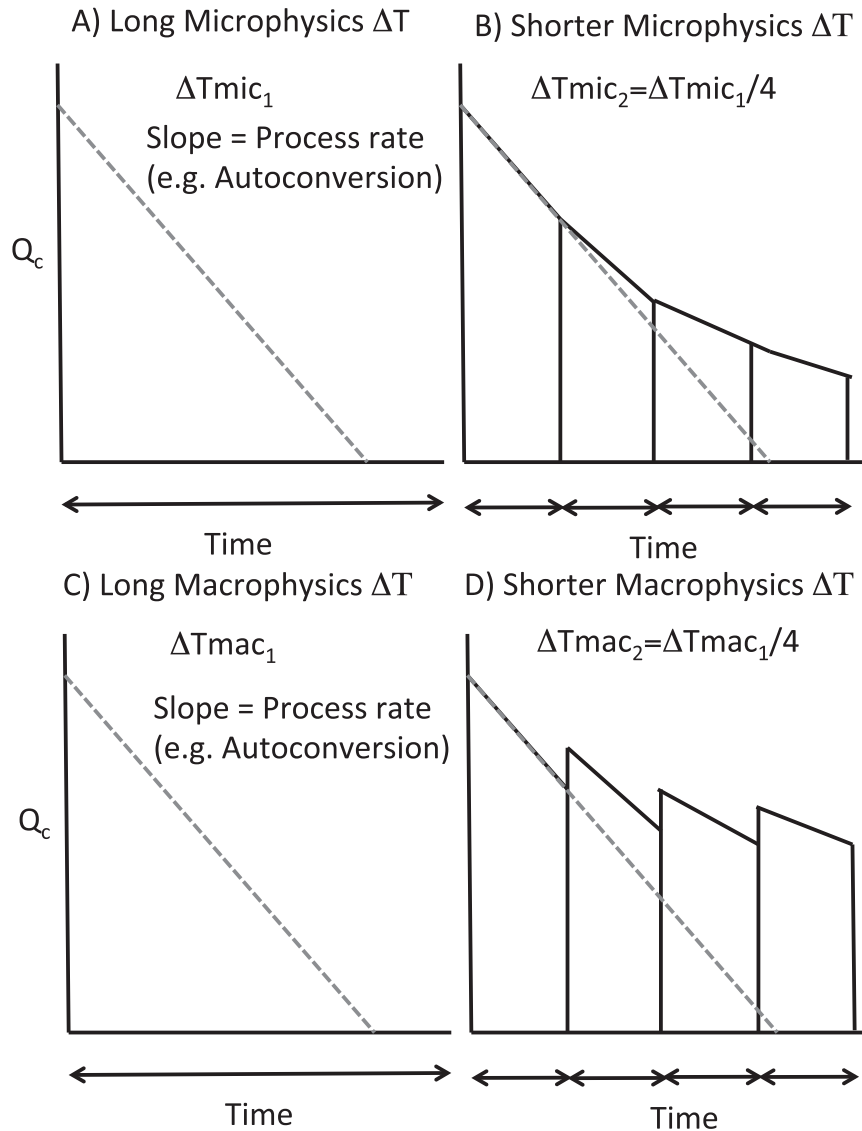


FIG. 1. Schematic of process rates (sloped lines) depleting liquid water (Q_c) over various time steps: (a) long microphysics, (b) short microphysics, (c) long macrophysics, and (d) short macrophysics. See text for details.

d. Sensitivity tests

We also explore single-column model simulations where the entire model physics time step has been shortened by a factor of 4 from 1200 to 300 s ($dt/4$) and simulations where a different macrophysics, CLUBB, is used (Bogenschutz et al. 2012). In the latter formulation macrophysics plus microphysics is substepped at four times (Mi1Ma4) because CLUBB requires a time step ≤ 300 s and the single-column model uses a 1200-s time step. All simulations except for those with CLUBB use the standard cloud macrophysics in CAM (Neale et al. 2010).

We also perform several global model simulations. We do this for MG1.5 and MG2 with Mi2Ma1 (base case) as well as MG2 with Mi2Ma2, Mi4Ma1, and Mi1Ma4. The latter three tests all have four microphysics substeps, with different numbers of macrophysics steps. Global simulations for each case are performed with year 2000 aerosol emissions, and year 1850 emissions, as described below. We also run CLUBB globally, and since the global model runs with 1800-s time steps we use Mi1Ma6 for this case.

The top-of-atmosphere (TOA) radiative imbalance is relatively small for all runs. The global simulations have a TOA radiative imbalance of between 0.2 and

TABLE 1. Description of runs used in this study.

Simulation	Micro steps (Mi)	Macro steps (Ma)	SCAM	Global (2000)	Global (1850)
MG1.5	2	1	Y	Y	Y
MG2	2	1	Y	Y	Y
MG2 dt/4	1	1	Y		
Mi1,4,8,16	1,4,8,16	1	Y		
Mi2Ma2	2	2	Y	Y	Y
Mi4Ma1	4	1	Y	Y	Y
Mi1Ma4	1	4	Y	Y	Y
CLUBB-Mi1Ma4	1	4	Y		
CLUBB-Mi1Ma6	1	6		Y	Y

2.3 W m^{-2} except for CLUBB-Mi1Ma6, which has a balance of 3.2 W m^{-2} . For such small imbalances in simulations with fixed sea surface temperatures (SSTs), the TOA imbalance is not expected to have significant impact on quantities such as ACI which are the focus of this paper. Therefore no tuning was required, and all simulations are run with the same parameter settings except as noted above.

e. Diagnostics

As stated in the introduction, we are interested in the effect of the different coupling strategies on the resulting microphysical state, process rates, and aerosol–cloud interactions. We will look at how the different microphysical couplings alter the basic cloud state in the simulations, by looking at the cloud fraction, liquid and ice mass, and precipitation. For global simulations, we will also examine cloud radiative properties that may change in response to changes in the microphysics and its coupling to the model.

We will also look at the microphysical process rates. This includes the accretion (Ac) and autoconversion (Au) rates, and their ratio (Ac/Au). These diagnostics were used by Gettelman et al. (2013) to evaluate the original version of the scheme (MG2008) relative to idealized process models, large eddy simulations, and observational estimates. The balance of cloud processes and cloud aerosol interactions have been shown to be sensitive to these changes.

In addition, we can track cases such as that represented in Fig. 1a when all condensate is depleted within a single step. In the microphysics code, when process rates are calculated, if the rates would deplete all condensate over a time step then they are adjusted to not “overdeplete” condensate, by simply scaling all the process rates by a value sufficient to bring the condensate to zero at the end of the time step. This ratio (a scaling factor) can be used as a diagnostic. When the scaling factor is 1, there are no limits applied to liquid process rates. When the scaling factor is less than 1, the process rates are being limited.

For metrics in global simulations, we will focus on cloud microphysical parameters (condensate and particle sizes) that affect the radiative properties of clouds. We will also look at the microphysical process rates, especially rain formation rates from accretion and autoconversion. We will examine the aerosol–cloud interactions (ACI) focusing on radiative properties of direct and indirect ACI.

f. Single-column test cases

In this work we will focus on two different single-column model cases. The Single Column Atmosphere Model (SCAM) runs the physical parameterization suite of CAM5 using a specified dynamical forcing framework for one column of the atmosphere. There is no horizontal advection of hydrometeors. The time step is 1200 s.

The first case is a drizzling stratocumulus cloud case from the Dynamics and Chemistry of Stratocumulus II (DYCOMS-II) experiment, case RF02, as described by Ackerman et al. (2009). This case has been extensively compared to large-eddy simulation (LES) models (Ackerman et al. 2009), and we show results from a single LES case (Bogenschutz et al. 2012) from the System for Atmospheric Modeling (SAM; Khairoutdinov and Randall 2003). This case includes relatively simple, constant forcing over 12 h. For some of the analyses (noted below) we extend this forcing to 48 h for better statistics. Specified drop number N_c for the LES is 55 cm^{-3} , very close to the value of 50 cm^{-3} assumed in SCAM simulations.

The second case is based upon observations of Arctic mixed-phase clouds from Barrow, Alaska, taken as part of the Atmospheric Radiation Measurement Program’s (ARM) Microphysics of Arctic Clouds Experiment (MPACE; Verlinde et al. 2007) in October 2004. The experiment featured a mix of deep and shallow clouds, as well as a high proportion of mixed-phase clouds. We will compare the results to several sets of in situ and ground-based remote sensing field observations. For the MPACE case, we average over a period from 5 to 8

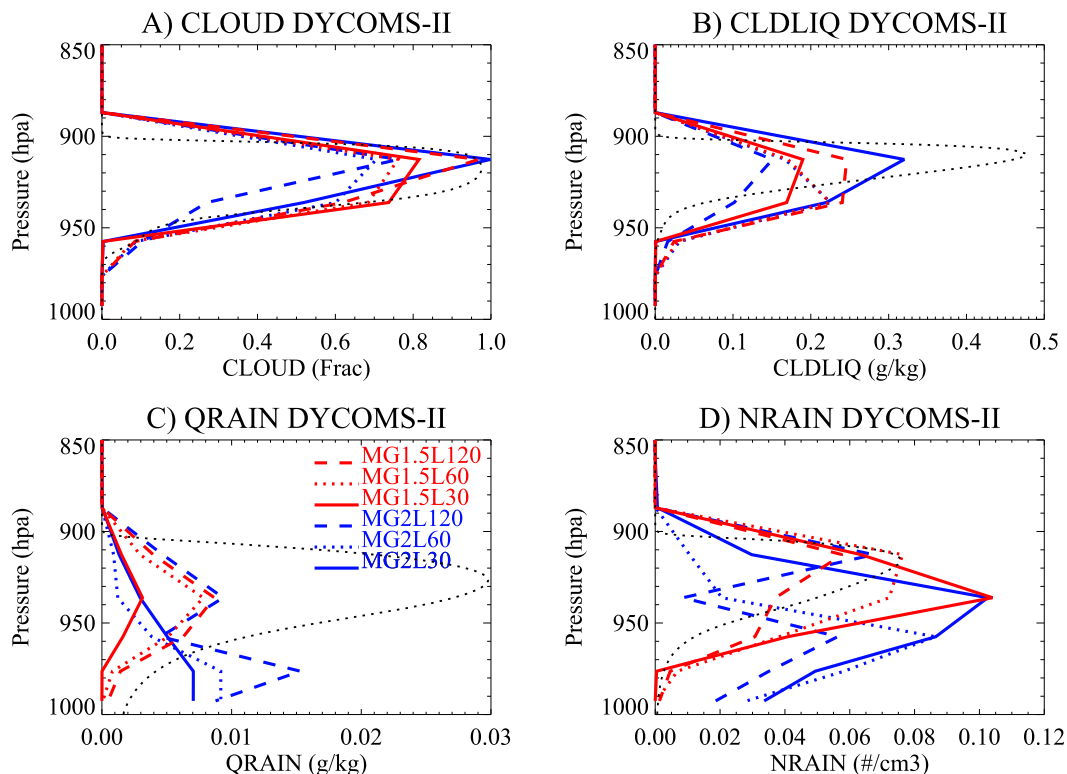


FIG. 2. Single-column simulation output for DYCOMS-II-RF02 case (averaged over hours 8–12 of 12 h) for (a) cloud fraction (CLOUD), (b) cloud liquid mixing ratio (CLDLIQ), (c) rain mixing ratio (QRAIN), and (d) rain number concentration (NRAIN) for different cases: MG1.5 (red) and MG2 (blue), with 30 levels (solid), 60 level (dotted), and 120 levels (dashed). Black dotted lines are averaged LES solutions for the case for the same proportion of the end of the simulation (4–6 h).

October 2004 when there were extensive and persistent low-level mixed-phase clouds. This case has been used previously to evaluate the microphysics by Gettelman et al. (2010).

Because the single-column model does not accurately simulate aerosols, we fix the number concentration of liquid drops and ice crystals in the single-column model simulations at 50 cm^{-3} and 5 L^{-1} (or 0.005 cm^{-3}) respectively. These values were chosen to be typical of the clean environments for marine and Arctic clouds in the DYCOMS-II and MPACE cases.

g. Global simulation configuration

In addition to single-column model simulations, we perform global simulations with CAM5 to understand the sensitivity of global climate to changes in the cloud microphysics. Global simulations are conducted for year 2000 concentrations of anthropogenic greenhouse gases (GHGs; chiefly CO_2 and CH_4), and climatological monthly mean ocean SSTs representing the period 1980–2000, repeated annually. Simulations are run for 6 years, with the last 5 years analyzed. Horizontal resolution is 1.9° latitude by 2.5° longitude on a Cartesian grid, with 30

levels from the surface to 3 hPa. By convention global model uses a time step of 1800 s at 1.9° resolution. We also perform test simulations with 0.23° latitude \times 0.31° horizontal resolution, 30 levels, and a 900-s time step. Simulations labeled “2000” use estimates of aerosol emissions from the year 2000. Simulations noted as 1850 are identical (same year 2000 boundary conditions for SSTs and GHGs), but they use aerosol emissions from 1850 estimates. The difference in these simulations represents the total radiative flux perturbation (RFP) due to anthropogenic aerosols.

3. Single-column results

Figure 2 illustrates the DYCOMS-II RF02 precipitating stratocumulus case with different vertical levels for MG2 and MG1.5 averaged over hours 8–12 of a steady 12-h simulation. LES results are from hours 4–6 of a 6-h simulation. The SCAM DYCOMS-II RF02 times were selected for a period when the model cases have a clear and stable stratiform cloud layer for an appropriate comparison with LES simulations. The timing is different in these SCAM simulations due to different

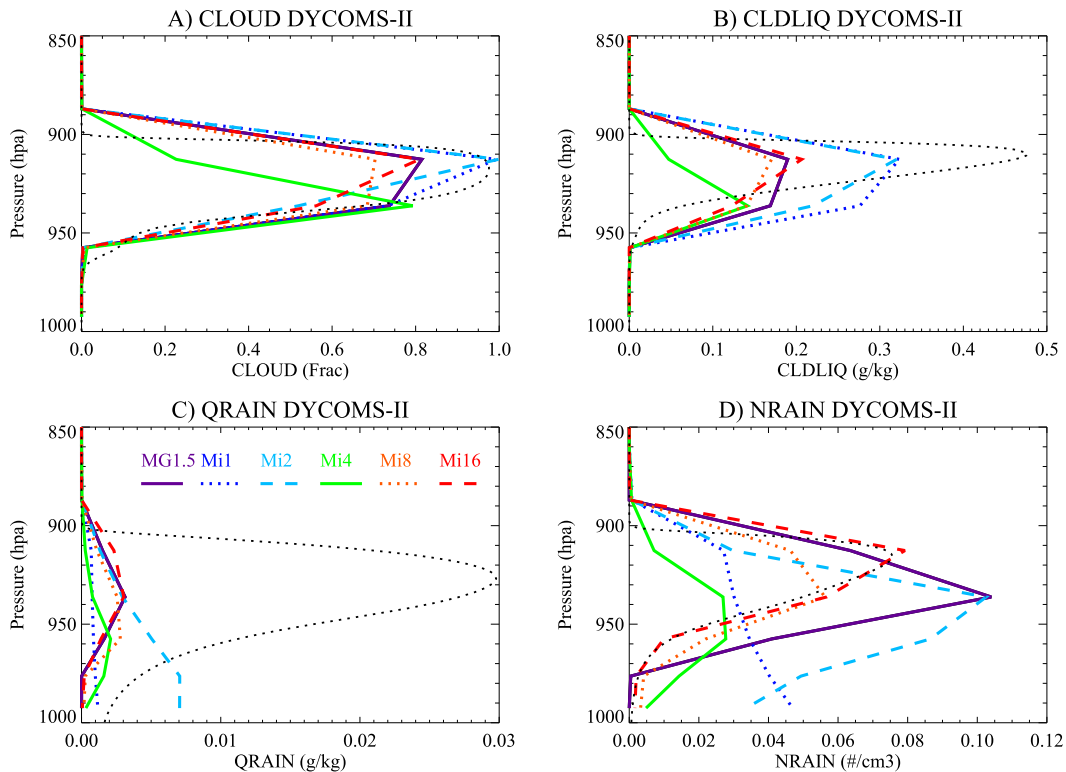


FIG. 3. Single-column simulation output for DYCOMS-II-RF02 case with MG2 and 30 levels for (a) cloud fraction (CLOUD), (b) cloud liquid mixing ratio (CLDLIQ), (c) rain mixing ratio (QRAIN), and (d) rain number concentration (NRAIN) for different cases: MG1.5 (purple solid), MG2 (other colors) with 1 (dark blue dotted), 2 (light blue dashed), 4 (green solid), 8 (orange dotted), and 16 (red dashed) microphysics substeps. Black dotted lines are averaged LES solutions for the case. The base case is Mi2 (light blue).

forcing (but still the same last $\frac{1}{3}$ of the simulation). We test 30 (base case), 60, and 120 levels, with the increase in levels simply halving the distance between levels. Figure 2a indicates that cloud fraction is sensitive to vertical resolution; however, all the simulations (MG1.5 and MG2, at all vertical levels) generate a peak cloud fraction of between 0.88 and 0.99 at approximately the same altitude range as the LES. L120 MG1.5 and MG2 seem to provide the best match to LES (cloud fraction and liquid amount). Figure 2b indicates the total liquid cloud mass, Fig. 2c the rain mass, and Fig. 2d the rain number concentration. Cloud drop number concentration is fixed at 50 cm^{-3} . Liquid cloud mass is sensitive to the vertical resolution (it varies by 50% in MG2 with vertical resolution). The peak value in MG2 is lower than the LES estimated peak value, and at a lower altitude for L60. Rain mass (Fig. 2c) is very sensitive to vertical resolution, particularly in MG2. The sensitivity of rain mass to vertical grid spacing in MG2 is likely related to substepping the sedimentation for numerical stability, which means precipitation may fall more than one grid cell without undergoing evaporation or other microphysical processes during the long (1200 s) model time step. Also note that

other parameterizations in SCAM may be sensitive to time step, such as vertical diffusion and macrophysics. Part I found that running MG2 in an offline driver caused decreases in rain rate for larger vertical spacing, but limited sensitivity for vertical grid spacings smaller than 200 m. Rain number (Fig. 2d) is also sensitive to resolution in MG2. There is a peak in rain number at cloud top for L120. We focus here on the microphysics, but the dynamical setup may also be an issue. For example, the boundary layer entrainment may be quite different in SCAM and the LES model, leading to a different LWP. In all of the DYCOMS-II cases, we have examined the limiter (QCRAT; not shown), which scales liquid mass process rates to prevent overdepletion (if there is no scaling, $\text{QCRAT} = 1$). The limiter is almost never active in these cases with appreciable liquid water. For different (lower) values of drop number with less liquid, these limiters are active for the DYCOMS-II case.

Figure 3 shows the effect of changing substeps in MG2, progressively increasing from 1 to 16 using the standard 30-level model configuration. The default is two substeps (Mi2). The Mi2 case corresponds to MG2L30 in Fig. 2. Peak cloud fraction (Fig. 3a) varies between 0.7 and 1.0.

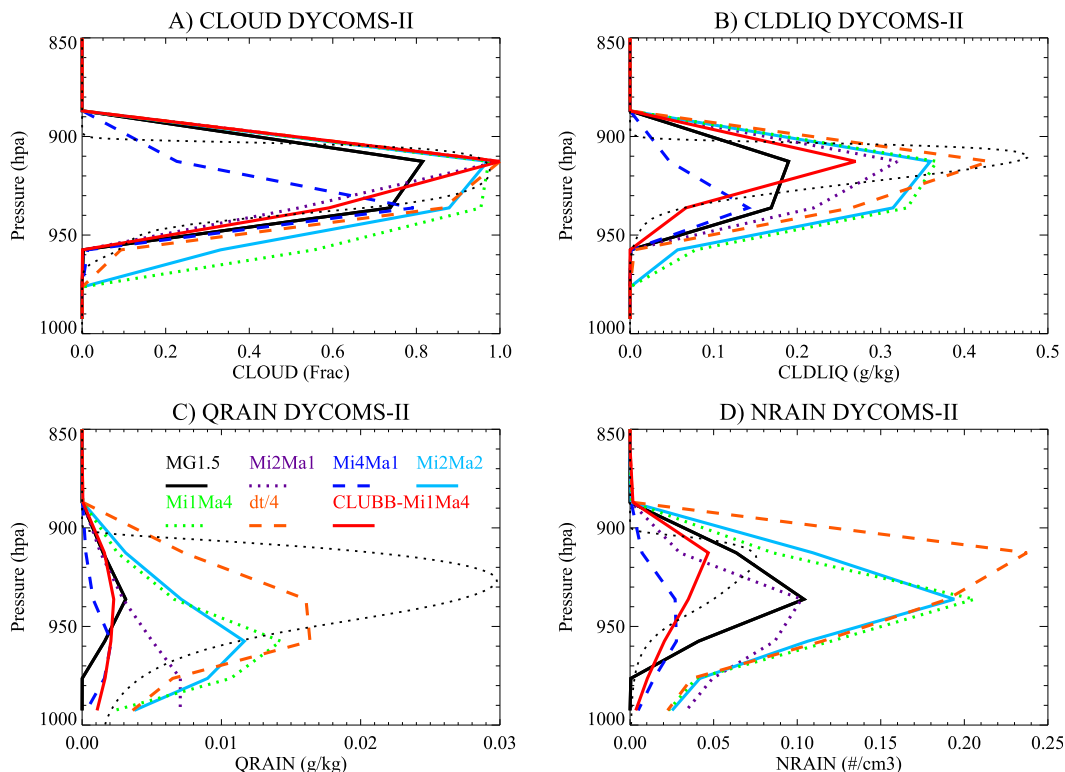


FIG. 4. Single-column simulation output for DYCOMS-II-RF02 case for (a) cloud fraction (CLOUD), (b) cloud liquid mixing ratio (CLDLIQ), (c) rain mixing ratio (QRAIN), and (d) limiting ratio on liquid process rates (QCRAT) for different cases: MG1.5 (black solid), MG2 (other colors) with 2 microphysics and 1 macrophysics substeps (Mi2Ma1; purple dotted), 4 microphysics and 1 macrophysics step (Mi4Ma1; dark blue dashed), 2 microphysics and 2 macrophysics substeps (Mi2Ma2; light blue solid), and 1 microphysics and 4 macrophysics substeps (Mi1Ma4; green dotted). Also shown are simulations with the entire 1200-s time step set to 300 s (dt/4; orange dashed) and a simulation using CLUBB macrophysics in an Mi1Ma4 configuration (CLUBB-Mi1Ma4; red solid). Black dotted lines are averaged LES solutions for the case.

Cloud liquid mass (Fig. 3b) is lower than LES estimates, and varies substantially between simulations with different substeps. The simulation with only a single substep (Mi1) has the most cloud mass. Since limiters are not active in the DYCOMS-II case, the sensitivity of cloud mass to substeps is not the same as hypothesized in Fig. 1. This may result from most of the condensation occurring on the first substep after the first macrophysics call. Rain mass does change substantially, becoming more like the LES (and MG1.5) at four substeps and higher (Fig. 3c). This is likely due to the reduced need for substepping sedimentation as the number of microphysical substeps is increased, since substepping sedimentation leads to precipitation falling multiple grid levels without undergoing evaporation as discussed above. Rain number (Fig. 3d) has a peaked structure above the ground for all cases except Mi1. The representation of rain appears better with a higher number of substeps, more consistent with LES.

Figure 4 illustrates results using four microphysics substeps, but with different configurations of the coupling

with macrophysics and microphysics as indicated in Table 1. In Fig. 4a, the cloud fraction peaks at 100% (completely overcast), except for MG1.5 (90%) and Mi4Ma1 (80%). As with other configurations, the cloud liquid mass (Fig. 4b) is smaller for MG1.5 and MG2-Mi4Ma1 but higher for Mi1Ma4, dt300, and CLUBB (a different macrophysics scheme, run with Mi1Ma4 configuration). The distribution of the rain mass peak above the surface (Fig. 4c) looks closer to LES for most of the simulations compared with Mi1 (Fig. 3c) or Mi2Ma1 (Fig. 4c). The other cases with multiple macrophysics steps (Mi1Ma4, Mi2Ma2, CLUBB, and dt300) provide a better representation of the rain structure compared to LES. Rain number (Fig. 4d) has a similar structure for all cases, but is lower in the Mi2Ma1 and Mi4Ma1 cases (higher with multiple macrophysics calls).

Figure 5 illustrates the ratio of accretion to autoconversion (Ac/Au), vertically averaged, for the DYCOMS-II RF02 case. The forcing has been extended from 6 to 48 h for better statistics. The ratio is calculated at each time

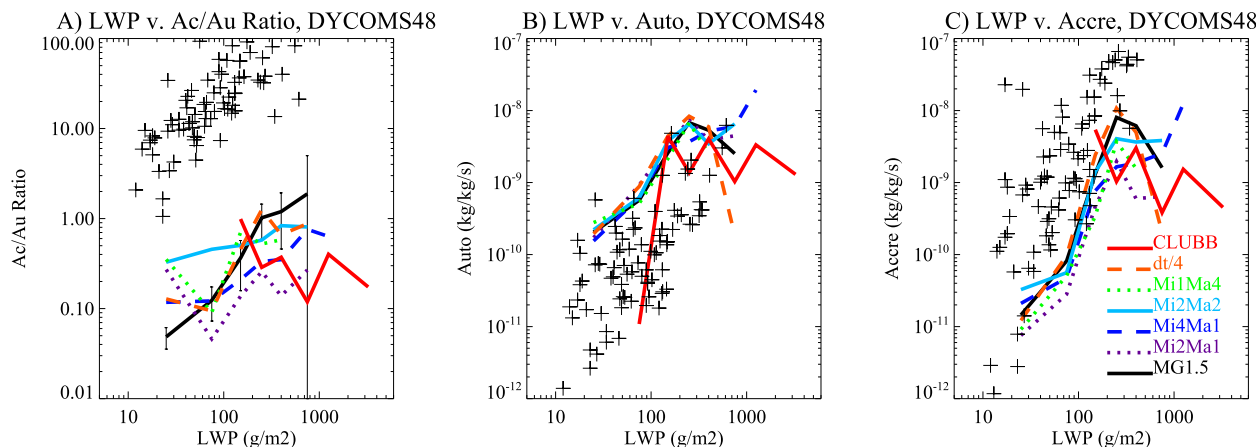


FIG. 5. Single-column simulation output for the DYCOMS-II-RF02 case of vertical averaged (a) accretion to autoconversion ratio (Ac/Au), (b) autoconversion, and (c) vertically averaged accretion. Averages of liquid water path (LWP) bins shown with standard deviation as error bars. MG1.5 (black solid), MG2 (other colors) with 2 microphysics and 1 macrophysics substeps (Mi2Ma1; purple dotted), 4 microphysics and one macrophysics step (Mi4Ma1; dark blue dashed), 2 microphysics and 2 macrophysics substeps (Mi2Ma2; light blue solid), and 1 microphysics and 4 macrophysics substeps (Mi1Ma4; green dotted). Also shown are simulations with the entire 1200s time step set to 300s (dt/4; orange dashed) and a simulation using CLUBB macrophysics in an Mi1Ma4 configuration (CLUBB-Mi1Ma4; red solid). For the DYCOMS-II case, estimates derived from observations from the VOCALS experiment shown as black crosses (see text for details).

and averaged, so the average of the ratio binned by LWP (Fig. 5a) is not the same as the ratio of the averages (Figs. 5b,c). Both MG1.5 (black solid) and MG2-Mi2Ma1 (purple dotted) are shown. Error bars (shown only for MG1.5) indicate that there is significant scatter in each bin, increasing for the largest LWP bins (where it swamps differences between simulations). The “observations” are estimates of process rates calculated with in situ aircraft measured particle size distributions from the VAMOS Ocean-Cloud-Atmosphere-Land Study (VOCALS) experiment in the southeast Pacific (Wood et al. 2011) using the method described by Wood (2005) and presented in Gettelman et al. (2013). In offline simulations in Part I, MG1.5 has small increases in the Ac/Au ratio as LWP increases, while MG2 has larger increases. The behavior is expected as prognostic rain allows it to build up over time, and accretion is sensitive to rain mass, while autoconversion is not. In the DYCOMS-II case, MG1.5 and MG2 (Mi2Ma1) are similar, with MG1.5 even having a higher Ac/Au ratio. Most of the other coupling cases (Mi4Ma1, Mi2Ma2, and Mi1Ma4) are similar in Fig. 5a. The dt/4 and CLUBB cases behave differently, with decreases in the Ac/Au ratio for $LWP > 100 \text{ cm}^{-3}$ driven by decreases in accretion (Fig. 5c). The simulated accretion rates are lower than the estimates from VOCALS, although the slope with LWP is similar. The difference in the ratio between observational estimates and the simulations is likely due to the fixed drop concentration (N_c) assumption with $N_c = 50 \text{ cm}^{-3}$. In a test, setting $N_c = 100 \text{ cm}^{-3}$ increased accretion and the Ac/Au ratio by an order of magnitude.

This makes some sense as the autoconversion rate will be significantly higher with low drop numbers, so fixing it may artificially alter process rates. We will return to a discussion of process rates with global simulations that do not fix drop number concentration.

Now we examine a more complex mixed-phase cloud case from MPACE (Verlinde et al. 2007). We have selected the period from 5 to 8 October 2004 when only low stratiform clouds are present, seen in Fig. 6 (dotted line) from observations. These data come from remote sensing retrievals of cloud fraction, liquid water content, and ice water content. The comparisons with SCAM in Fig. 6 show a high cloud layer that is seen only sporadically in the observations with passage of synoptic-scale systems and fronts. Despite the excess high clouds, there is too little simulated ice mass (Fig. 6b) by large factors. This high cloud layer in the MPACE cases is a feature of the very active ice nucleation scheme and fixed crystal number (which creates the same number of crystals if any ice is present). In simulations with variable crystal number and low aerosol concentrations (or ice nucleation fixed as a function of temperature), this layer is not present. It is thus a feature of the fixed crystal number simulations. The ice content (IWC; Fig. 6b) and liquid content (LWC; Fig. 6c) are similar in most of the simulations. All simulations have low ice content, with CLUBB slightly higher (Fig. 6b). The LWC (Fig. 6c) is similar in most simulations, and compares well to the observations. Note that a dt/4 run with MG1.5 instead of MG2 looks very similar to the dt/4 simulations shown in Fig. 6 with MG2, indicating that in this simulation, the

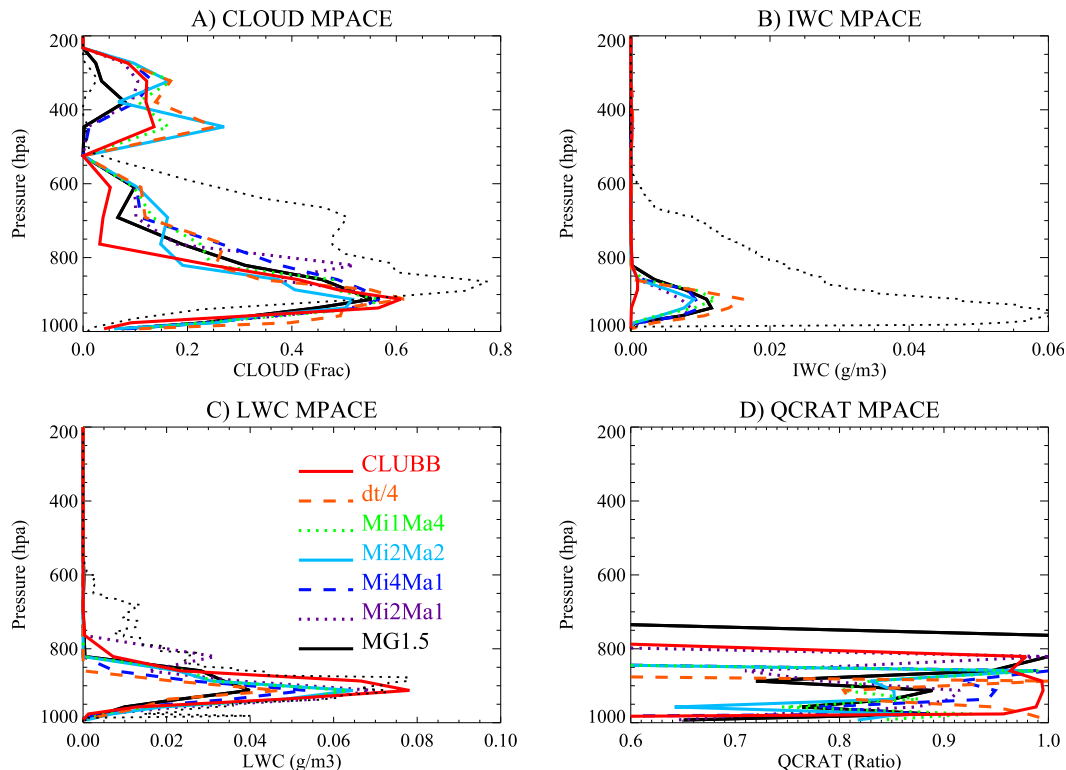


FIG. 6. Single-column simulation output for MPACE case for 5–8 Oct 2004 for (a) cloud fraction (CLOUD), (b) ice water content (IWC), (c) liquid water content (LWC), and (d) limiting ratio on liquid process rates (QCRAT) for different cases (when liquid exists): MG1.5 (black solid), MG2 (other colors) with 2 microphysics and 1 macrophysics substeps (Mi2Ma1; purple dotted), 4 microphysics and one macrophysics step (Mi4Ma1; dark blue dashed), 2 microphysics and 2 macrophysics substeps (Mi2Ma2; light blue solid), and 1 microphysics and 4 macrophysics substeps (Mi1Ma4; green dotted). Also shown are simulations with the entire 1200-s time step set to 300 s (dt/4; orange dashed) and a simulation using CLUBB macrophysics in an Mi1Ma4 configuration (CLUBB-Mi1Ma4; red solid). Black dotted lines are remote sensing retrievals for the same time interval.

coupling of the other physical processes (not microphysics) is dominating the results.

There is a wide spread of how often the process rate limiter is active (Fig. 6d; QCRAT) across the simulations. Recall this is the scaling on the total liquid mass mixing ratio tendency (sum of the process rates): a value of 1 indicates no limiter, and 0.5 indicates the process rates are scaled by 50%. At 900 hPa, the lower LWP cases (like Mi1Ma4 and dt/4) seem to have the lowest value of the limiter (largest effect) around 0.8 while CLUBB (highest LWP) has the least impact (highest value) of the limiter, at nearly 1.0 throughout the cloud layer.

A different method of substepping in the MPACE case is to use different microphysics substeps with one macrophysics step (Fig. 7). Simulations using the different substeps with MG2 (from 1 to 16) also indicate a reduction of the effect of the limiter (Fig. 7d) at 1000–850 hPa with higher LWC (Fig. 7c). The limiter effect decreases (higher QCRAT) with more substeps (Fig. 7d),

even if the LWP decreases with more substeps. For Mi4 or higher (Mi8, Mi16), the limiter is ≥ 0.95 in the cloud layer.

The reason the limiter is active in the MPACE case can be determined by looking at the microphysical process rates. Figure 8 shows the time averaged process rates for liquid in the microphysics. The dominant process rates are the rapid vapor deposition onto ice and snow and evaporation of liquid, and these cause the limiter to be invoked. At lower levels, the accretion of liquid onto snow is also important. In global simulations, these processes tend to occur in colder regions (high latitudes and winter seasons) with supercooled liquid as in the MPACE case illustrated here.

An examination (not shown) of the relationship between accretion and autoconversion for the MPACE case, similar to Fig. 5 for DYCOMS-II, indicates very similar results: increases in accretion and autoconversion with LWP, but generally higher autoconversion, in contrast to observations. However, since these are liquid

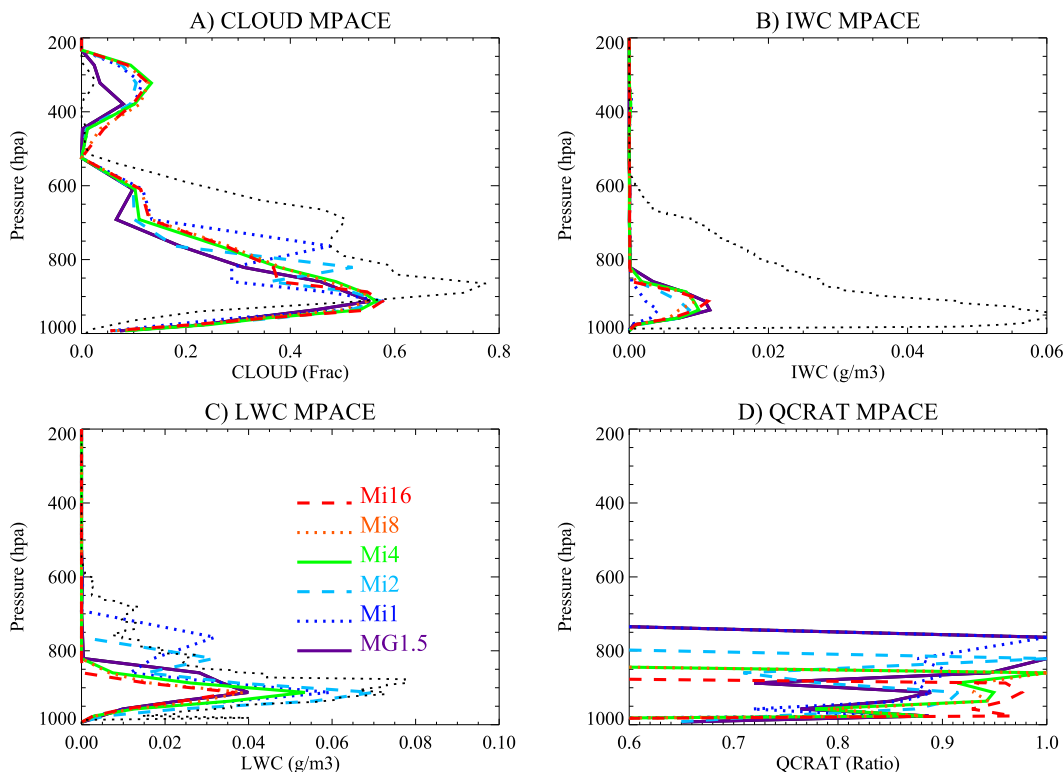


FIG. 7. Single-column simulation output for MPACE case averaged for 5–8 Oct 2004 for (a) cloud fraction (CLOUD), (b) IWC, (c) LWC, and (d) limiting ratio on liquid process rates (QCRAT) for different cases: MG1.5 (purple solid), MG2 (other colors) with 1 (dark blue dotted), 2 (light blue dashed), 4 (green solid), 8 (orange dotted), and 16 (red dashed) substeps. The base case is Mi2 (light blue). Black dotted lines are remote sensing retrievals for the same time interval.

process rates for a mixed-phase case, interpretation of the results is difficult.

In summary, then, which configuration is “better”? The number of substeps is not a tuning knob; the correct solution to the governing equations is given by the limit as the number of substeps goes to infinity. Deviation from this constitutes numerical error. The impact of the process rate limiter is one way to gauge this effect. The limiter on process rates is a significant factor in cold regions with supercooled water. This results from lower liquid amounts, and also from the importance of the vapor deposition (Bergeron) process that depletes water onto ice and snow. Cases with more microphysics substeps (Mi4 and higher, including CAM-CLUBB) seem to have less impact of the limiter, which is still moderate (values are 0.8 to 1.0, indicating a maximum 20% effect). CLUBB produces more LWP in the MPACE case, which is more realistic compared to observations, but it produces little ice. The MG2 simulations have more LWC than MG1.5 in the MPACE case, and more cloud mass in the DYCOMS-II case. Cases in which the macrophysics (condensation) is substepped more than once in each time step (Mi2Ma2, Mi1Ma4, and CLUBB) do seem to

reproduce the structure of rain better and have higher LWP in the DYCOMS-II case. There is no particular case with multiple macrophysics steps that matches observations closely in the MPACE case, and there is generally too little ice in all simulations at low levels, and anomalous ice at upper levels.

4. Global results

We now explore global simulation results of some of the sensitivity tests (Fig. 9). Figure 9 compares annual zonal means to quantities retrieved from satellites where available. Comparisons are based on climatological annual means from observations to attempt to minimize sampling biases. The uncertainties and different sensitivities of retrievals are significant. The current Cloud Feedback Model Intercomparison Project (CFMIP) Operational Simulator Package (COSP; Bodas-Salcedo et al. 2011) and its implementation in CAM (Kay et al. 2012) contain only one microphysical quantity [Moderate Resolution Imaging Spectroradiometer (MODIS) cloud-top effective radius], thus we use traditional geophysical retrievals compared to model geophysical quantities

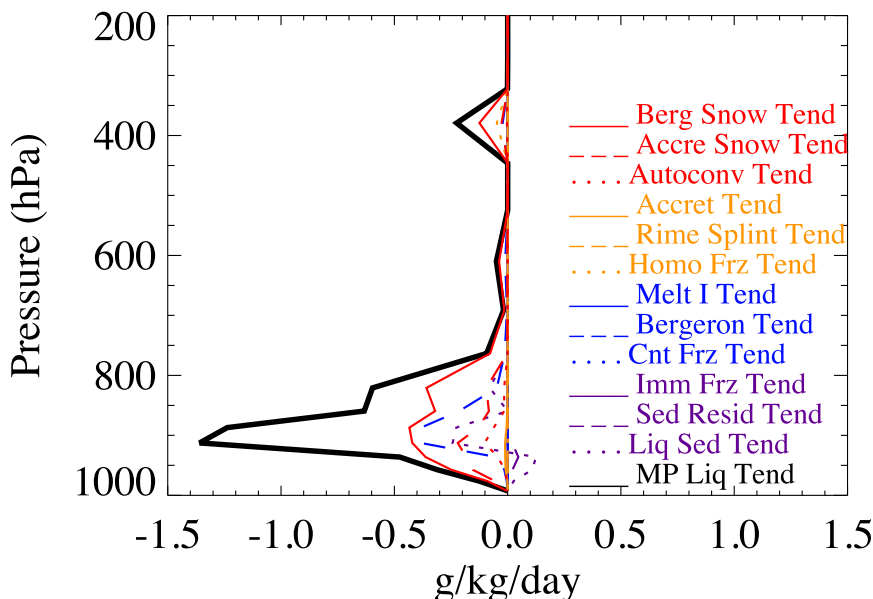


FIG. 8. Single-column simulation output of liquid tendencies for MPACE case for MG2 (averaged over 5–8 Oct 2004). Total tendency in black. Dotted and solid lines are different tendencies as noted on the figure. Dominant tendencies are the evaporation of liquid and the vapor deposition onto snow (Berg Snow: red solid) and ice (Bergeron: dashed blue), with accretion (red dashed) also factoring into the total process rates.

where available. Uncertainties in the observations even at the monthly mean scale are 15%–30% and estimates are included in Table 2. Uncertainties in cloud forcing come from calibration uncertainties and determination of clear-sky values (Loeb et al. 2009). Advanced Very High Resolution Radiometer (AVHRR) uncertainties are discussed by Han et al. (1994) and include calibration, viewing geometry, and size distribution assumptions. Global Precipitation Climatology Project (GPCP) precipitation estimates have been found to have uncertainties of 20% for individual region monthly means relative to gauge data, but with a potential low bias of 15% (Krajewski et al. 2000). MODIS cloud-top retrievals (King et al. 2003) have significant uncertainties related to variations within a scene, and the presence of thin clouds above. Comparisons to the simulations are difficult due to cloud-top gradients in drop sizes, so we also use in situ ranges of drop size for clean (C) and polluted (P) conditions [see Gettelman et al. (2008) for details]. We do not report observational estimates for ice size (REI) and number (NI) due to retrieval uncertainties. We do not report observations for liquid and ice water path (LWP and IWP) because these quantities in the model are the radiative values, not microphysical values (as shown elsewhere in this study), and are not directly comparable to satellite water path observations.

Globally, Fig. 9 reveals several differences in mean state climate between MG2 (dark blue dotted) and

MG1.5 (purple solid). The differences are quantitatively highlighted in global means in Table 2. Cloud forcing in the shortwave (SW; Fig. 9a) and longwave (LW; Fig. 9b) is stronger in MG2 than MG1.5 for both the storm tracks and the tropics. The cloud forcing is too strong globally relative to observations (Table 2). The bias originates mainly in the tropics and results from the parameterization of radiatively active cloud water within convective clouds, which is beyond the scope of this work. This increase in forcing at high latitudes in MG2 is an improvement, due to ice clouds with smaller ice crystal sizes (Fig. 9f).

Column drop number (Fig. 9c) is lower than MG1.5 in the Northern Hemisphere for all simulations with MG2. Cloud-top drop radius (Fig. 9e) is similar in MG2. Cloud-top properties are defined as the radius of clouds in the uppermost model grid box containing cloud of that phase at each time step. Comparisons to observation in Fig. 9e do not account for different sensitivity of satellites and the vertically uniform cloud properties in each model layer. This is an example where we know there is a substantial mismatch between observations and simulations, but better microphysical retrievals and satellite simulators for them are not yet available.

Figure 9 also illustrates global results for the different sensitivity tests. The only substantial differences are decreases in cloud top ice size (Fig. 9f) with the sensitivity tests of more than two substeps for microphysics.

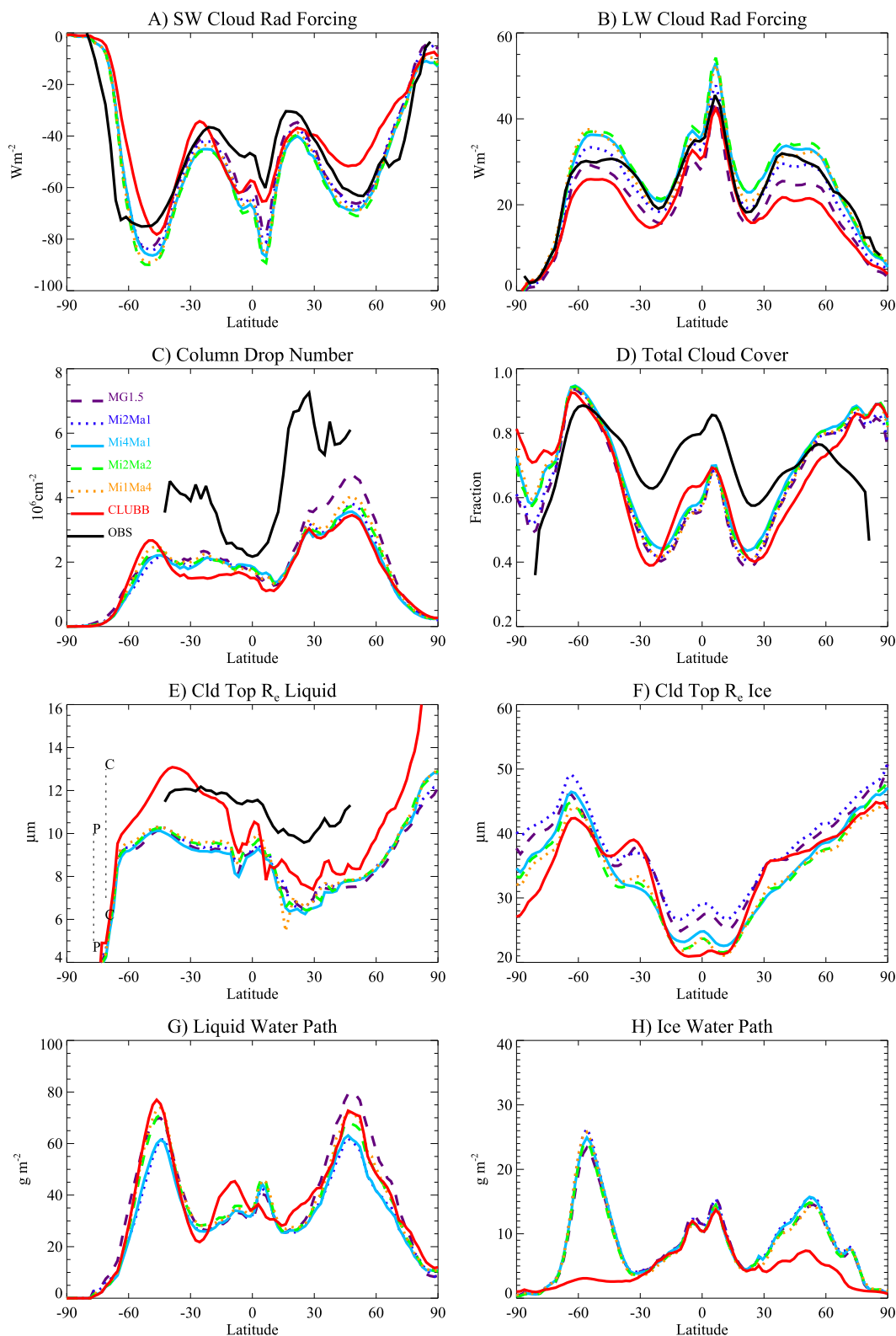


FIG. 9. Zonal means for MG1.5 (purple dashed) and MG2 sensitivity tests: Mi2Ma1 (base MG2; dark blue dotted), Mi4Ma1 (light blue solid), Mi2Ma2 (green dashed), and Mi1Ma4 (orange dotted) as well as MG2 with CLUBB macrophysics (Mi1Ma6; red solid) for (a) SW and (b) LW cloud radiative forcing (v. CERES, solid), (c) column drop number (v. AVHRR, solid), (d) total cloud cover (v. CLOUDSAT, solid), (e) cloud-top liquid size (v. MODIS, solid), (f) cloud-top ice size, (g) LWP over ocean, and (h) ice water path.

TABLE 2. Global mean statistics with year 2000 aerosol emissions: radiative imbalance at top of atmosphere (R_{ToA}), shortwave (SWCE) and longwave (LWCE) cloud radiative forcing and clouds and the Earth's Radiant Energy System (CERES) observations, column drop number (CNC) and AVHRR observations, cloud-top effective radius for liquid (REL) vs MODIS observations, cloud-top ice size (REL), liquid water path (LWP), ice water path (IWP), cloud-top ice number (NI), and precipitation (PREC) vs GPCP.

Run	R_{ToA} (W m^{-2})	SWCE (W m^{-2})	LWCE (W m^{-2})	CNC (10^6 cm^{-2})	REL (10^{-6} m)	REL (10^{-6} m)	LWP (g m^{-2})	IWP (g m^{-2})	NI (L^{-1})	PREC (mm day^{-1})
MG1.5	0.2	-52.6	22.8	2.29	8.41	33.7	45.0	9.4	9.1	3.00
MG2-Mi2Ma1	1.9	-54.4	26.4	2.02	8.52	34.7	39.3	9.7	9.4	2.96
MG2-Mi4Ma1	2.3	-57.1	29.7	2.01	8.28	31.0	39.6	9.4	11.4	2.89
MG2-Mi2Ma2	1.6	-58.4	30.4	2.07	8.51	30.3	42.9	9.1	15.5	2.87
MG2-Mi1Ma4	1.6	-56.4	28.7	2.13	8.60	30.5	43.7	9.0	17.4	2.90
CLUBB	3.2	-47.5	21.9	1.88	9.84	31.7	40.2	5.8	24.9	2.73
OBS		-48.5	27.2	4.01	10.5					2.67
Uncert (%)		15%	15%	25%	25%					20%

These contribute to slightly larger magnitude of the cloud forcing (Figs. 9a,b). The CLUBB simulation, run with six substeps for an 1800-s global model time step, has a very different representation of the ice cloud closure assumptions (Bogenschutz et al. 2013) and much smaller IWP (Fig. 9h), contributing to weaker cloud forcing (Figs. 9a,b). CLUBB also has higher effective liquid sizes (Fig. 9e). Note that none of these tests was retuned: all cases have the same values for common parameters that affect the LW (auto-conversion size threshold for ice) and SW (critical relative humidity threshold for low cloud formation). There is no critical relative humidity threshold for low clouds in CAM-CLUBB.

Figure 10 illustrates the changes to the mass of precipitation using the new prognostic precipitation in MG2. There are significant (30%–50%) decreases in peak rain mass, mostly near the surface. This seems to be the opposite effect from the DYCOMS-II simulations (Fig. 2) where rain mass was higher in MG2 near the surface than MG1.5, at least for the stratus cloud in the DYCOMS-II case. This shows that SCAM cases are not always good proxies for overall climatological behavior. There are also decreases in snow mass at higher altitudes (~ 700 hPa) in the tropics in particular. High-latitude and high-altitude snow mass (which is important for and included in the radiation scheme) does not change very much. Snow number (not shown) does increase. Since snow is included in the radiation code, this contributes to the optically thicker clouds in MG2.

Surface precipitation decreases slightly (-5% in the zonal mean) with MG2 between 30°S and 30°N over the tropical and subtropical oceans. Global precipitation decreases by $\sim 1\%$ from 3.00 to 2.96 mm day^{-1} (consistent with a slightly different energy imbalance). There is little change in the partitioning between stratiform and convective precipitation with the new MG2 scheme.

MG1.5 and MG2 simulations have also been run at 0.23° horizontal resolution ($\sim 25 \text{ km}$). The cloud macrophysics is sensitive to horizontal resolution (Bacmeister et al. 2014), with clouds decreasing at higher resolution. The differences between MG2 and MG1.5 shown in Figs. 9 and 10 are similar at higher resolution, but MG2 changes less than MG1.5 (MG2 is less sensitive to increasing resolution). No qualitative differences between low and high resolution are seen in fields presented in Table 2 and Fig. 9. Diagnostics for the advection of prognostic precipitation are currently in development; this will be investigated in future work.

We have performed simulations for preindustrial aerosol emissions. Differences between the year 2000 emissions and 1850 emissions are indicated in Table 3. With MG2, there is a clear reduction in the total

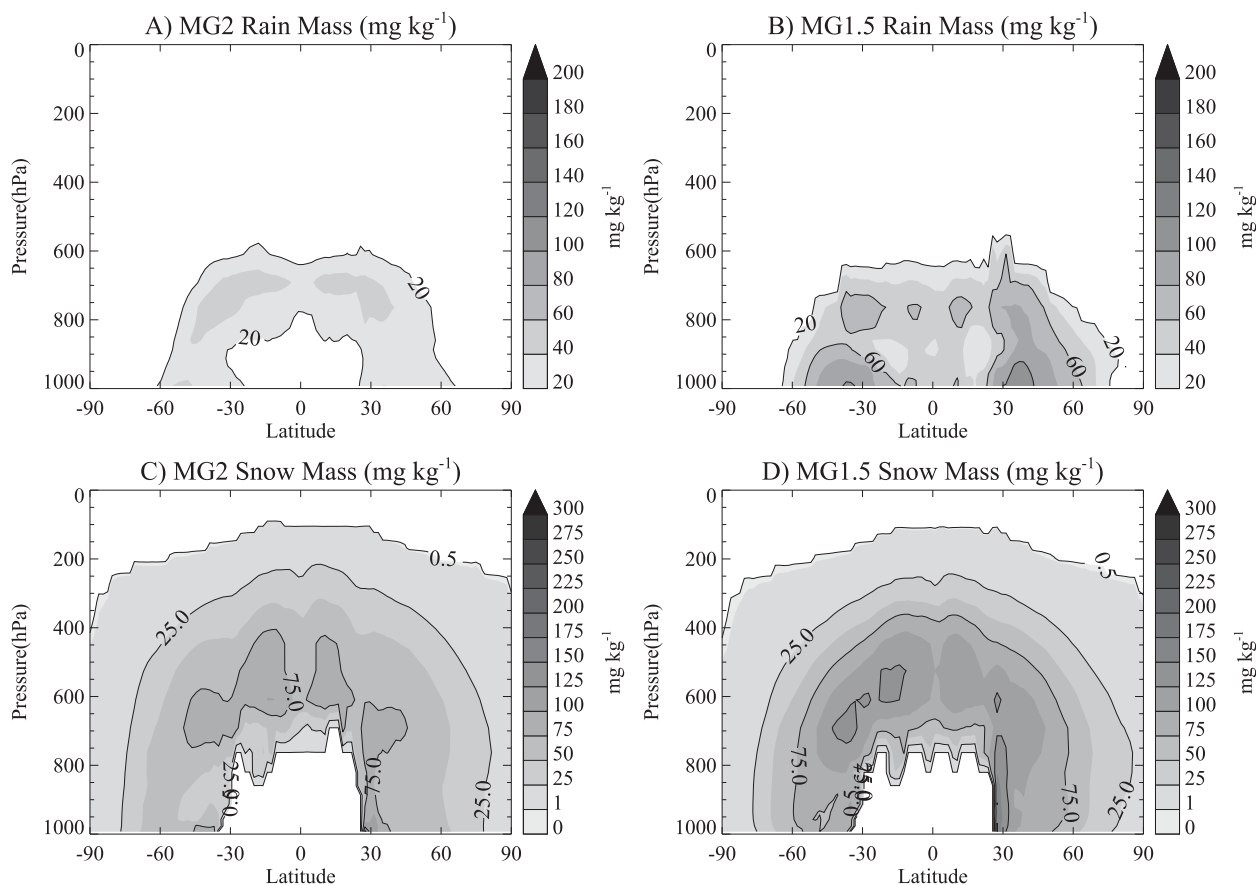


FIG. 10. Zonal mean annual (a),(b) rain and (c),(d) snow mass mixing ratio from (left) MG2 and (right) MG1.5.

radiative flux perturbation (ΔR). The direct effect estimated using a diagnostic calculation from dual calls to the radiation code, with and without aerosols, is similar (~ -0.04 to -0.09 W m^{-2} except for CLUBB) and small, so most of this is a change in the indirect effect (ACI) resulting from reductions to the change in cloud radiative effect or cloud forcing (ΔCRE) by between 2%–33% (except for CLUBB), depending on the substepping. Note that except for CLUBB, the change in cloud forcing is associated with a smaller change in LWP between preindustrial and present. The largest change in ACI (ΔCRE) occurs when more than one call is made to the cloud macrophysics (Mi2Ma2 and Mi1Ma4). Also note that CLUBB includes ACI in the shallow convective regime, which may account for the larger total ACI effects.

We have also evaluated these estimates using the alternative methodology for estimating ACI from Ghan (2013). Ghan (2013) calculates ACI based on ΔCRE estimated neglecting clear-sky aerosol scattering and absorption. The slightly different definition from Ghan (2013), which uses estimates of radiative effects of clouds in the absence of clear-sky aerosols, increases ACI by

$\sim -0.2 \text{ W m}^{-2}$. This is illustrated in Table 4. Note that the direct effects in Table 4 are the same as in Table 3. The results using this method are qualitatively the same: the lowest ACI occur with the Mi2Ma2 case. The quantitative reduction in ACI with MG2 using this method is 2%–24%. It appears that substepping microphysics only (Mi2Ma1 and Mi4Ma1) does not affect ΔR as much as substepping macrophysics (Mi1Ma4 and Mi2Ma2). The smallest ACI values are seen for the Mi2Ma2 case, when both macrophysics and microphysics are substepped (Mi2Ma2).

Figure 11 indicates the locations where the aerosol–cloud interactions have changed between MG1.5 and MG2 (Mi2Ma1) using the change in cloud radiative effect as a metric for ACI. The reduction occurs throughout the planet. There are large reductions in cloud forcing changes in the tropics, particularly around Southeast Asia, and in the North Pacific. The sign of the effect over eastern China has also changed to slightly positive, and that over North America and Europe to neutral or negative. The emissions changes are the same between the simulations. There are ACI reductions in the stratocumulus regions off the western coasts of continents, particularly off the California

TABLE 3. Radiative flux perturbation from MG1.5 and MG2: 2000 – 1850 aerosol emissions differences in W m^{-2} (except ΔLWP); ΔR is the change in TOA flux (LW + SW), ΔCRE is the change in cloud radiative effect (also called cloud forcing: LW + SW), and its component changes are ΔSWCRE (shortwave) and ΔLWCRE (longwave). Also shown are the percent changes in liquid water path (ΔLWP) and the change in aerosol direct effect (ΔDE) estimated using all-sky radiative calculations with and without aerosols.

Run	ΔR	ΔCRE	ΔSWCRE	ΔLWCRE	ΔLWP (%)	ΔDE
MG1.5	-1.23	-0.93	-1.15	+0.22	+8.0	-0.08
MG2-Mi2Ma1	-1.08	-0.76	-0.91	+0.15	+5.8	-0.07
MG2-Mi4Ma1	-1.06	-0.91	-1.15	+0.23	+6.9	-0.09
MG2-Mi2Ma2	-0.90	-0.62	-0.96	+0.34	+5.6	-0.08
MG2-Mi1Ma4	-0.82	-0.71	-0.73	+0.03	+4.8	-0.04
CLUBB-Mi1Ma6	-1.40	-1.13	-1.07	-0.06	+4.9	-0.02

coast. The largest effects in MG2 are over oceanic regions, especially the North Pacific.

The reason for the reductions can be seen in process rates, similar to the single-column simulations (Fig. 5). Figure 12 illustrates the accretion/autoconversion ratios as a function of LWP for the different sensitivity simulations including MG1.5 (purple) and MG2 (dark blue). We have averaged over 60°S – 60°N , but results are similar if smaller regions are used. Relative to the single-column model case (Fig. 5), accretion rates are half an order of magnitude higher (Fig. 12c) and autoconversion rates half an order of magnitude or so lower (Fig. 12b), resulting in significant increases in the Ac/Au ratio (Fig. 12a). The difference with Fig. 5 is partly due to the variable drop number in global simulations (Fixed in SCAM). As with Fig. 5, the average of the LWP binned ratio in Fig. 12a is not the same as the ratio of the averages in each LWP bin (Figs. 12b,c). Process rate estimates from observations during the VOCALS experiment in the southeast Pacific (Wood et al. 2011) are also shown (as in Fig. 5). MG2 results are in better agreement with estimates from observations, although autoconversion remains high. In MG1.5 (purple in Fig. 12), the accretion to autoconversion ratio (Fig. 12a) is an order of magnitude lower than in the other simulations because of higher autoconversion (Fig. 12b) at higher LWP and lower accretion (Fig. 12c) at any LWP. The difference is despite using the same process formulations for accretion and autoconversion in all simulations. Sensitivity tests are also shown in the plot. Note that the cases with multiple calls to cloud macrophysics (Mi2Ma2, Mi1Ma4, and CLUBB) have lower autoconversion at low and high LWP. CLUBB seems to behave differently because of higher accretion at low LWP (Fig. 12c). There is not a one-to-one correspondence between these relationships and the magnitude of the aerosol–cloud interactions, but it appears that the simulations with lower ACI (Table 3), such as Mi2Ma2 and Mi1Ma4, feature rapid increases in the accretion to autoconversion ratio at $\text{LWP} < 100 \text{ cm}^{-3}$ (Fig. 12a), higher accretion in the LWP range of 50 – 500 cm^{-3} (Fig. 12c), and lower autoconversion (Fig. 12b)

at $\text{LWP} > 200 \text{ cm}^{-3}$. Note that CLUBB (red in Fig. 12) has higher accretion but a shallower slope, and it starts to decrease at high LWP.

One major difference between CAM-CLUBB and the CAM5 suite of simulations is that in CAM-CLUBB ACI are considered in both shallow cumulus and stratiform cloud, whereas for CAM5 they just occur in stratiform cloud.

Implementing prognostic precipitation does have a computational cost. There is also a cost for the advection of precipitation. Substepping of microphysics and macrophysics requires running parts of the code multiple times. Table 5 illustrates relative performance for the same configuration on the same computer system (the Yellowstone system at the NCAR Wyoming Supercomputing Center). The cost estimates do not include the advection of precipitation (expected to be an addition 2%–4% in any substepped configuration). MG2 in the standard configuration (Mi2Ma1) at $1.9^\circ \times 2.5^\circ$ horizontal resolution is about 1% more expensive than MG1.5. Running the microphysics twice more (Mi4Ma1) increases run time by 3%, indicating that running MG2 takes $\sim 1.5\%$ of the model run time. Running the macrophysics twice (Mi2Ma2) increases the model run time by another 10% or so. The Mi1Ma4 configuration is

TABLE 4. Radiative flux perturbation from MG1.5 and MG2: 2000 – 1850 aerosol emissions. Differences in W m^{-2} using the methodology of Ghan (2013); ΔR is the total radiative flux perturbation. Direct effects (DE) are estimated using the difference between top of atmosphere flux, and the same flux without clear-sky aerosols in the calculation. Aerosol–cloud interactions (ACI) are the cloud effects estimated again with fluxes that do not include clear-sky aerosol and ΔAlbedo is the change due to changes in surface properties (clear-sky shortwave fluxes without aerosols).

Run	ΔR	ΔDE	ΔACI	ΔAlbedo
MG1.5	-1.23	-0.08	-1.16	-0.15
MG2-Mi2Ma1	-1.08	-0.07	-0.98	-0.10
MG2-Mi4Ma1	-1.06	-0.09	-1.14	+0.14
MG2-Mi2Ma2	-0.90	-0.09	-0.89	+0.04
MG2-Mi1Ma4	-0.82	-0.04	-0.97	+0.04
CLUBB-Mi1Ma6	-1.40	-0.02	-1.53	-0.01

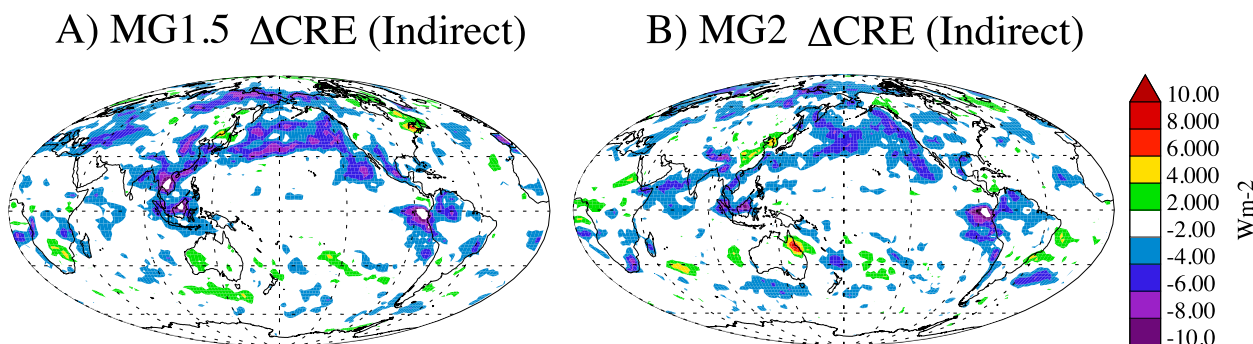


FIG. 11. Change in cloud radiative effect (CRE) between years 2000 and 1850 simulations for (a) MG1.5 and (b) MG2 in W m^{-2} .

slightly more efficient (three more macrophysics steps are only a 21% increase over Mi4Ma1, or 7% per macrophysics step). The limited cost of more substeps likely occurs because the microphysics does not perform calculations on substeps when no condensate is present.

5. Summary and conclusions

Single-column and global results were presented for a new implementation of the MG2008 microphysics in the Community Earth System Model (CESM). The microphysics is embedded in the model using a flexible framework that allows different substeps between microphysics and macrophysics (large-scale condensation) to be run. MG2 has skill overall similar to that of MG1.5 in reproducing single-column cases for stratiform clouds (DYCOMS-II), but there are differences between SCAM and LES solutions. These differences between SCAM and LES solutions may result from dynamical feedbacks not related to microphysics. There are some problems with overactive ice nucleation in the single-column model in a mixed-phase case (MPACE) for both MG1.5 and MG2, and most of the configurations have too little liquid water. This might indicate continued problems with Arctic clouds, and it is a significant issue that needs addressing. The application of the liquid process rate limiter in these situations (mixed-phase clouds with small amounts of liquid) is a good diagnostic of potential problems with the rapid process of vapor deposition onto ice and snow with the associated evaporation of supercooled liquid. Substepping reduced the need for the limiter, but shorter time steps did not.

We have investigated different combinations of substepping microphysics and macrophysics down to time steps of just over a minute in the single-column model. Simulations with more than two substeps for the macrophysics in MG2 are closer to LES results with higher LWP (Fig. 4). This is evident in the vertical structure of rain mass for the DYCOMS-II case. With long time

steps, rain mass increases downward toward the surface monotonically because precipitation can fall multiple vertical levels without undergoing evaporation. With more than one macrophysics substep rain can evaporate below cloud, and peak precipitation mass occurs within cloud or near cloud base, more similar to the LES. Thus, use of two or more macrophysics substeps with MG2 is desirable. In the MPACE case, MG2 has more LWC than MG1.5, in better agreement with retrievals. All simulations have too little IWC for MPACE.

As expected, prognostic precipitation in the new microphysics results in a significant increase in accretion relative to autoconversion in the global simulations. In global simulations, averaged accretion increases modestly, and the accretion to autoconversion ratio is nearly an order of magnitude higher, compared to results with diagnostic precipitation. This is not seen in single-column model simulations, but SCAM may be influenced by the fixed drop number assumption in the single-column model simulations. These changes in results using prognostic versus diagnostic precipitation occur because of the difference in the process rates. The process rate changes are resolution-independent consequences of prognostic precipitation that has not often been considered, and occur even when advection of precipitation is not important.

In global simulations, the mean climate state changes only slightly with the introduction of the new microphysics scheme. The biggest changes are a reduction in ice water path, increases in storm track liquid water path and a slight increase in gross cloud forcing. MG2 seems to produce optically thicker clouds than MG1.5, related perhaps to reductions in autoconversion relative to accretion, and the changes in prognostic precipitation. The atmospheric loading of precipitation is reduced but snow number increases, and there is a small change in precipitation flux to the surface. Note that a decrease in globally averaged precipitation in steady state is only possible if surface evaporation and atmospheric radiative cooling increase. Liquid precipitation is affected

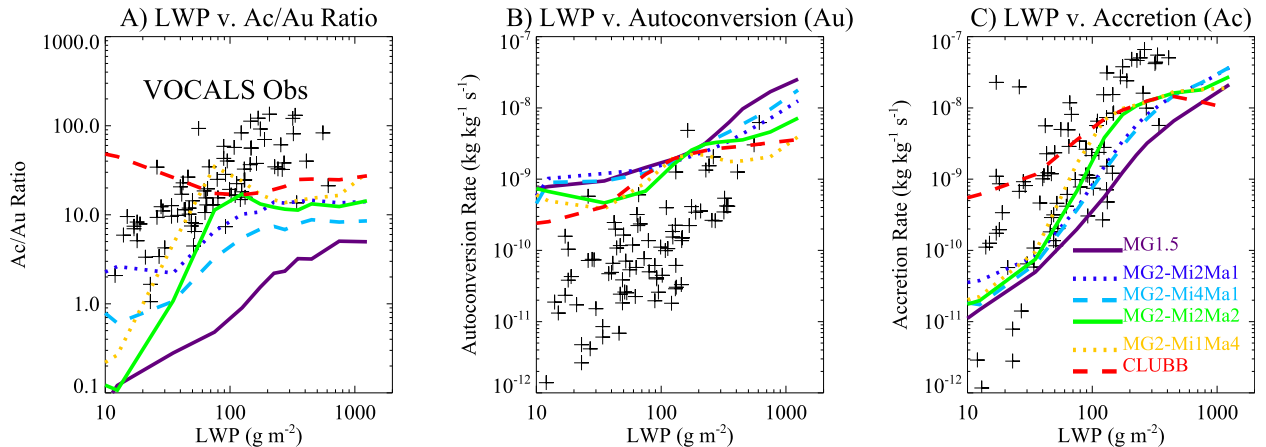


FIG. 12. The 60°S–60°N (a) ratio of accretion to autoconversion, (b) autoconversion rate, and (c) accretion rate from MG1.5 (purple solid), MG2-Mi2Ma1 (dark blue dotted), MG2-Mi4Ma1 (light blue dashed), MG2-Mi2Ma2 (green solid), MG2-Mi1Ma4 (yellow dotted), and CLUBB-Mi1Ma6 (red dashed). Estimates derived from observations from the VOCALS experiment shown as black crosses (see text for details).

more than ice. Liquid precipitation is not input to the radiation in CAM, so this does not change the radiative balance of the atmosphere much, but implies a slightly stronger hydrologic cycle with MG2 and prognostic precipitation, and more optically thick clouds. In exploratory high-resolution simulations, MG2 does not seem highly sensitive to horizontal resolution between 25 and 200 km and MG2 is less sensitive to changes in resolution than MG1.5.

The aerosol–cloud interactions are particularly sensitive to the treatment of precipitation and the substepping, even at coarse horizontal resolutions where horizontal advection is not important. Prognostic precipitation lowers the ACI by 2%–33% compared to diagnostic precipitation. Larger changes occur with multiple macrophysical and microphysical substeps, with Mi2Ma2 reducing the effect by 33%. The reductions in ACI occur significantly in the tropics, especially in South and Southeast Asia. The vertical structure of precipitation is different with prognostic precipitation and substepping. This leads to different process rates, especially accretion. The mechanism appears to be decreases in autoconversion rates at large liquid water paths and increases in accretion at moderate LWP, leading to increases in the effects of accretion in the simulations. This occurs particularly for the cases with substeps in the large-scale condensation (macrophysics).

Similar to the analysis of Golaz et al. (2011), ACI are sensitive to the microphysical process rates. In the simulations in Golaz et al. (2011), the process rates themselves (autoconversion) were tuned, and this modified both the radiative imbalance directly, as well as the impact of aerosols. In these simulations there was no tuning, as the changes in substepping did not affect the

radiative imbalance (which remains within 0.7 W m^{-2} for all simulations), but the substepping changes do affect the process rates such as autoconversion and the top-of-atmosphere flux change (ΔR ; Table 3). It remains to be seen if the different balance of clouds also affects climate feedbacks in CAM5, as in the GFDL model analyzed by Golaz et al. (2013).

This work indicates that microphysical process rates matter significantly for the treatment of cloud–aerosol interactions. These results confirm hypotheses that the ratio of accretion to autoconversion is important for the balance of precipitation processes. This work also highlights the importance of mixed-phase processes, and notes that the rapid vapor deposition onto ice and snow with evaporation of liquid is difficult to represent at long time scales where condensation creates water rapidly and vapor deposition depletes it. For cold regions of the planet, including the storm tracks, which are important for cloud feedbacks and climate sensitivity, it is important to correctly simulate the balance of clouds by continuing to improve the representation of mixed-phase clouds. These regions are also sensitive to ice nucleation. Finally, the autoconversion representation in the simulations seems to indicate that

TABLE 5. Timing relative to MG2-Mi2Ma1 base case for global experiments with the same configuration.

Run	Relative time
MG1.5	0.989
MG2-Mi2Ma1	1.000
MG2-Mi4Ma1	1.030
MG2-Mi2Ma2	1.151
MG2-Mi1Ma4	1.243

autoconversion rates are substantially larger at low LWP than estimates based on observations. This might result from an inability to resolve the vertical structure of cloud water. It might also be related to the underlying difficulty in representing drop growth from collision/coalescence in bulk microphysics schemes such as MG (all versions). This remains a subject for future work.

Acknowledgments. This work was partially supported by NASA NNX09AJ05G, U.S. DOE ASR DE-SC0006702, and U.S. DOE ASR DE-SC0005336, sub-awarded through NASA NNX12AH90G. The work was also supported by the NSF Science and Technology Center for Multiscale Modeling of Atmospheric Processes (CMMAP), managed by Colorado State University under Cooperative Agreement ATM-0425247. Caldwell's efforts were funded by DOE's Earth System Modeling program and were performed under the auspices of DOE by Lawrence Livermore National Laboratory under Contract DE-AC52-07NA27344. Thanks to R. Neale for comments.

REFERENCES

- Abdul-Razzak, H., and S. J. Ghan, 2000: A parameterization of aerosol activation: 2. Multiple aerosol types. *J. Geophys. Res.*, **105** (D5), 6837–6844, doi:10.1029/1999JD901161.
- Ackerman, A. S., and Coauthors, 2009: Large-eddy simulations of a drizzling, stratocumulus-topped marine boundary layer. *Mon. Wea. Rev.*, **137**, 1083–1110, doi:10.1175/2008MWR2582.1.
- Albrecht, B. A., 1989: Aerosols, cloud microphysics, and fractional cloudiness. *Science*, **245**, 1227–1230, doi:10.1126/science.245.4923.1227.
- Bacmeister, J. T., M. F. Wehner, R. B. Neale, A. Gettelman, C. Hannay, P. H. Lauritzen, J. M. Caron, and J. E. Truesdale, 2014: Exploratory high-resolution climate simulations using the Community Atmosphere Model (CAM). *J. Climate*, **27**, 3073–3099, doi:10.1175/JCLI-D-13-00387.1.
- Bodas-Salcedo, A., and Coauthors, 2011: COSP: Satellite simulation software for model assessment. *Bull. Amer. Meteor. Soc.*, **92**, 1023–1043, doi:10.1175/2011BAMS2856.1.
- Bogenschutz, P. A., A. Gettelman, H. Morrison, V. E. Larson, D. P. Schanen, N. R. Meyer, and C. Craig, 2012: Unified parameterization of the planetary boundary layer and shallow convection with a higher-order turbulence closure in the Community Atmosphere Model: Single-column experiments. *Geosci. Model Dev.*, **5**, 1407–1423, doi:10.5194/gmd-5-1407-2012.
- , —, —, —, C. Craig, and D. P. Schanen, 2013: Higher-order turbulence closure and its impact on climate simulation in the Community Atmosphere Model. *J. Climate*, **26**, 9655–9676, doi:10.1175/JCLI-D-13-00075.1.
- Bretherton, C. S., and S. Park, 2009: A new moist turbulence parameterization in the Community Atmosphere Model. *J. Climate*, **22**, 3422–3448, doi:10.1175/2008JCLI2556.1.
- Gettelman, A., and H. Morrison, 2014: Advanced two-moment bulk microphysics for global models. Part I: Off-line tests and comparison with other schemes. *J. Climate*, **28**, 1268–1287, doi:10.1175/JCLI-D-14-00102.1.
- , —, and S. J. Ghan, 2008: A new two-moment bulk stratiform cloud microphysics scheme in the NCAR Community Atmosphere Model (CAM3). Part II: Single-column and global results. *J. Climate*, **21**, 3660–3679, doi:10.1175/2008JCLI2116.1.
- , and Coauthors, 2010: Global simulations of ice nucleation and ice supersaturation with an improved cloud scheme in the Community Atmosphere Model. *J. Geophys. Res.*, **115**, D18216, doi:10.1029/2009JD013797.
- , H. Morrison, C. R. Terai, and R. Wood, 2013: Microphysical process rates and global aerosol–cloud interactions. *Atmos. Chem. Phys. Discuss.*, **13**, 11 789–11 825, doi:10.5194/acpd-13-11789-2013.
- Ghan, S. J., 2013: Technical note: Estimating aerosol effects on cloud radiative forcing. *Atmos. Chem. Phys.*, **13**, 9971–9974, doi:10.5194/acp-13-9971-2013.
- , and Coauthors, 2011: Droplet nucleation: Physically-based parameterizations and comparative evaluation. *J. Adv. Model. Earth Syst.*, **3**, M10001, doi:10.1029/2011MS000074.
- Golaz, J.-C., V. E. Larson, and W. R. Cotton, 2002: A PDF-based model for boundary layer clouds. Part I: Method and model description. *J. Atmos. Sci.*, **59**, 3540–3551, doi:10.1175/1520-0469(2002)059<3540:APBMFB>2.0.CO;2.
- , M. Saltzman, L. J. Donner, L. W. Horowitz, Y. Ming, and M. Zhao, 2011: Sensitivity of the aerosol indirect effect to subgrid variability in the cloud parameterization of the GFDL atmosphere general circulation model AM3. *J. Climate*, **24**, 3145–3160, doi:10.1175/2010JCLI3945.1.
- , L. W. Horowitz, and H. Levy, 2013: Cloud tuning in a coupled climate model: Impact on 20th century warming. *Geophys. Res. Lett.*, **40**, 2246–2251, doi:10.1002/grl.50232.
- Han, Q., W. B. Rossow, and A. A. Lacis, 1994: Near-global survey of effective droplet radii in liquid water clouds using ISCCP data. *J. Climate*, **7**, 465–497, doi:10.1175/1520-0442(1994)007<0465:NGSOED>2.0.CO;2.
- Kärcher, B., J. Hendricks, and U. Lohmann, 2006: Physically based parameterization of cirrus cloud formation for use in atmospheric models. *J. Geophys. Res.*, **111**, D01205, doi:10.1029/2005JD006219.
- Kay, J. E., and Coauthors, 2012: Exposing global cloud biases in the Community Atmosphere Model (CAM) using satellite observations and their corresponding instrument simulators. *J. Climate*, **25**, 5190–5207, doi:10.1175/JCLI-D-11-00469.1.
- Khairoutdinov, M. F., and Y. Kogan, 2000: A new cloud physics parameterization in a large-eddy simulation model of marine stratocumulus. *Mon. Wea. Rev.*, **128**, 229–243, doi:10.1175/1520-0493(2000)128<0229:ANCPPI>2.0.CO;2.
- , and D. A. Randall, 2003: Cloud resolving modeling of the ARM summer 1997 IOP: Model formulations, results, uncertainties and sensitivities. *J. Atmos. Sci.*, **60**, 607–625, doi:10.1175/1520-0469(2003)060<0607:CRMOTA>2.0.CO;2.
- King, M. D., and Coauthors, 2003: Cloud and aerosol properties, precipitable water, and profiles of temperature and water vapor from MODIS. *IEEE Trans. Geosci. Remote Sens.*, **41**, 442–457, doi:10.1109/TGRS.2002.808226.
- Krajewski, W. F., G. J. Ciach, J. R. McCollum, and C. Bacotiu, 2000: Initial validation of the Global Precipitation Climatology Project monthly rainfall over the United States. *J. Appl. Meteor.*, **39**, 1071–1086, doi:10.1175/1520-0450(2000)039<1071:IVOTGP>2.0.CO;2.
- Liu, X., J. E. Penner, S. J. Ghan, and M. Wang, 2007: Inclusion of ice microphysics in the NCAR Community Atmosphere

- Model version 3 (CAM3). *J. Climate*, **20**, 4526–4547, doi:10.1175/JCLI4264.1.
- , and Coauthors, 2012: Towards a minimal representation of aerosol direct and indirect effects: Description and evaluation in the Community Atmosphere Model CAM5. *Geosci. Model Dev.*, **5**, 709–739, doi:10.5194/gmd-5-709-2012.
- Loeb, N. G., B. A. Wielicki, D. R. Doelling, G. L. Smith, D. F. Keyes, S. Kato, N. Manalo-Smith, and T. Wong, 2009: Towards optimal closure of the earth's top-of-atmosphere radiation budget. *J. Climate*, **22**, 748–766, doi:10.1175/2008JCLI2637.1.
- Lohmann, U., J. Feichter, C. C. Chuang, and J. Penner, 1999: Prediction of the number of cloud droplets in the ECHAM GCM. *J. Geophys. Res.*, **104** (D8), 9169–9198, doi:10.1029/1999JD900046.
- Milbrandt, J., and M. Yau, 2005: A multimoment bulk microphysics parameterization. Part I: Analysis of the role of the spectral shape parameter. *J. Atmos. Sci.*, **62**, 3051–3064, doi:10.1175/JAS3534.1.
- Morrison, H., and A. Gettelman, 2008: A new two-moment bulk stratiform cloud microphysics scheme in the NCAR Community Atmosphere Model (CAM3). Part I: Description and numerical tests. *J. Climate*, **21**, 3642–3659, doi:10.1175/2008JCLI2105.1.
- , J. A. Curry, and V. I. Khvorostyanov, 2005: A new double-moment microphysics parameterization for application in cloud and climate models. Part I: Description. *J. Atmos. Sci.*, **62**, 1665–1677, doi:10.1175/JAS3446.1.
- Neale, R. B., J. H. Richter, and M. Jochum, 2008: The impact of convection on ENSO: From a delayed oscillator to a series of events. *J. Climate*, **21**, 5904–5924, doi:10.1175/2008JCLI2244.1.
- , and Coauthors, 2010: Description of the NCAR Community Atmosphere Model (CAM5.0). NCAR Tech. Rep. NCAR/TN-486+STR, 274 pp.
- Park, S., and C. S. Bretherton, 2009: The University of Washington shallow convection and moist turbulence schemes and their impact on climate simulations with the Community Atmosphere Model. *J. Climate*, **22**, 3449–3469, doi:10.1175/2008JCLI2557.1.
- Platnick, S., and S. Twomey, 1994: Determining the susceptibility of cloud albedo to changes in droplet concentration with the Advanced Very High Resolution Radiometer. *J. Appl. Meteor.*, **33**, 334–347, doi:10.1175/1520-0450(1994)033<0334:DTSOCA>2.0.CO;2.
- Posselt, R., and U. Lohmann, 2008: Introduction of prognostic rain in ECHAM5: Design and single column model simulations. *Atmos. Chem. Phys.*, **8**, 2949–2963, doi:10.5194/acp-8-2949-2008.
- , and —, 2009: Sensitivity of the total anthropogenic aerosol effect to the treatment of rain in a global climate model. *Geophys. Res. Lett.*, **36**, L02805, doi:10.1029/2008GL035796.
- Quaas, J., and Coauthors, 2009: Aerosol indirect effects—General circulation model intercomparison and evaluation with satellite data. *Atmos. Chem. Phys.*, **9**, 8697–8717, doi:10.5194/acp-9-8697-2009.
- Solomon, S., D. Qin, M. Manning, Z. Chen, M. Marquis, K. B. Averyt, M. Tignor, and H. L. Miller, Eds., 2007: *Climate Change 2007: The Physical Science Basis*. Cambridge University Press, 996 pp.
- Thompson, G., P. R. Field, R. M. Rasmussen, and W. D. Hall, 2008: Explicit forecasts of winter precipitation using an improved bulk microphysics scheme. Part II: Implementation of a new snow parameterization. *Mon. Wea. Rev.*, **136**, 5095–5115, doi:10.1175/2008MWR2387.1.
- Twomey, S., 1977: The influence of pollution on the shortwave albedo of clouds. *J. Atmos. Sci.*, **34**, 1149–1152, doi:10.1175/1520-0469(1977)034<1149:TIOPOT>2.0.CO;2.
- Verlinde, J., and Coauthors, 2007: The Mixed-Phase Arctic Cloud Experiment. *Bull. Amer. Meteor. Soc.*, **88**, 205–221, doi:10.1175/BAMS-88-2-205.
- Walters, D. N., and Coauthors, 2014: The Met Office Unified Model Global Atmosphere 4.0 and JULES Global Land 4.0 configurations. *Geosci. Model Dev.*, **7**, 361–386, doi:10.5194/gmd-7-361-2014.
- Wood, R., 2005: Drizzle in stratiform boundary layer clouds. Part II: Microphysical aspects. *J. Atmos. Sci.*, **62**, 3034–3050, doi:10.1175/JAS3530.1.
- , and Coauthors, 2011: The VAMOS Ocean–Cloud–Atmosphere–Land Study Regional Experiment (VOCALS-REx): Goals, platforms, and field operations. *Atmos. Chem. Phys.*, **11**, 627–654, doi:10.5194/acp-11-627-2011.
- Zhang, G. J., and N. A. McFarlane, 1995: Sensitivity of climate simulations to the parameterization of cumulus convection in the Canadian Climate Center general circulation model. *Atmos.–Ocean*, **33**, 407–446, doi:10.1080/07055900.1995.9649539.